

# X-ray specs for solar cells

**Tamzin Lafford**, European Synchrotron Radiation Facility, Grenoble, France, & **Richard Bytheway** & **Daniel Bright**, Jordan Valley Semiconductors UK Ltd., Durham, UK

## ABSTRACT

Solar cell performance depends on material quality, as well as on the architecture of the cell. In the search for higher-performing cells, an ability to visualize the bulk and surface quality of the material is an advantage; to do this non-destructively, even in-line, is even better. It would be good to have X-ray vision to look inside, would it not? X-ray diffraction imaging (XRDI) does just that. Images are obtained of the distortions caused by crystal defects, and quantitative measures of the lattice deformation are available. In this paper the results obtained on a commercially available XRDI tool are compared with those from a large-scale public research facility.

## Introduction

Consider, for example, p-type homojunction solar cells. When fabricated with electronics-grade Czochralski-grown silicon (Cz-Si), cells achieve typical PV conversion efficiencies of 19%. The same architecture made with multicrystalline silicon (mc-Si) yields ~15–17%. An advancing competitor to Cz-Si is ‘mono-like’ silicon (also known as *quasi-monocrystalline silicon*), grown on industrial scales by directional solidification on a bed of high-quality seed crystals. Mono-like Si is faster and cheaper to manufacture than Cz-Si, and PV conversion efficiencies are now reaching ~18% in industrial processes.

It is fairly easy to identify a multicrystalline Si wafer or solar cell just by looking at it – the way the different crystalline orientations reflect the light (with or without surface treatments) reveals the different centimetric grains, even if one cannot classify all of them. Distinguishing a mono-like sample from a Czochralski sample is less obvious – and in either case, the outside appearance cannot tell you what the internal structure is like. Yet what is inside makes a significant difference to the performance of the finished cell, and localized defects may even be catastrophic, causing electrical breakdown or leading to wafer breakage during module construction.

“The diffraction image of a sample indicates the crystal defects that are present and where they are located.”

This is where X-ray vision has an advantage over visible light microscopy or even electron microscopy. While conventional inspection techniques can reveal defects on the surface following

## Bragg's Law: $n\lambda = 2d\sin\theta$

where  $n$  is an integer,  $\lambda$  is the wavelength of the X-rays,  $d$  is the spacing between lattice planes of a given orientation, and  $\theta$  is the angle of diffraction.

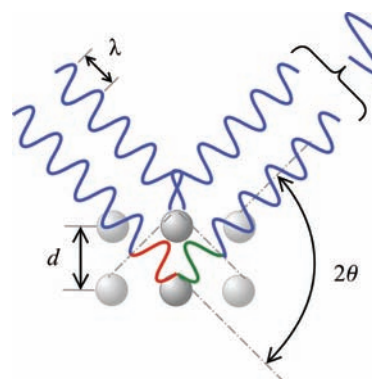


Figure 1. Derivation of Bragg's Law, for which W.H. and W.L. Bragg won the Nobel prize for physics in 1915, and illustration of X-ray diffraction from atomic planes. Constructive interference takes place when the path difference of the waves reflected from atomic planes differs by a whole number of wavelengths.

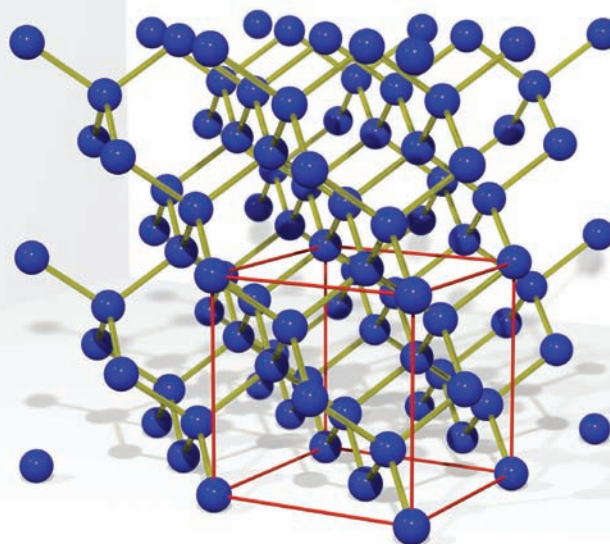


Figure 2. Crystal structure of silicon. The blue balls represent the positions of the Si atoms, and the yellow sticks the chemical bonds between them. The red outline represents a unit cell (face-centred cube).

particular surface treatment of small samples, X-rays can pass through the silicon; straightforward radiography (the same technique as used in hospitals for looking at broken bones inside the body) can be applied to the inspection of mechanical parts and electronic components.

But X-rays have an additional talent. Catch them at the right angle, and the planes of atoms in the silicon cause the X-ray beam to *diffract* according to Bragg's Law (see Figs. 1 and 2). This opens up a different type of imaging for crystalline samples, on a much finer scale and with the ability to look beyond the surface, with no special requirements as regards sample preparation. Where the 3D organization of the atoms in the crystal is near perfect, the resultant diffracted beam shows a uniform distribution of intensity. Defects such as dislocations, grain boundaries and precipitates deform the crystal locally and give *contrast* in the image, with different defects having characteristic 'signatures'. Thus the diffraction image of a sample indicates the crystal defects that are present and where they are located. Many types of defect can be highly detrimental to final PV performance, as can be demonstrated by light beam induced current (LBIC) or microwave photoconductance decay ( $\mu$ -PCD) mapping, for example.

X-ray diffraction imaging (XRDI, also known as *X-ray [diffraction] topography*) was developed in the 1950s and 1960s using standard laboratory X-ray tubes, and was, somewhat belatedly, key in the development of the growth of high-quality single crystals for the microelectronics industry. The advent of synchrotrons – special large facilities producing extremely high-intensity, quasi-coherent X-ray beams with very low divergence – extended the range of possibilities, in particular with regard to the exposure time, the accessible spatial resolution, and the scope for detailed quantitative analysis. However, for a wide variety of inspection-type applications, commercially available, simple-to-operate lab-based tools provide practical solutions.

Both approaches have their advantages. In this paper, XRDI images of samples of silicon wafers and solar cell structures (fabricated by the CEA-INES) obtained using the Jordan Valley (JV) QC-TT, fitted with a sealed tube X-ray source, are compared with images taken using beamline BM05 at the European Synchrotron Radiation Facility (ESRF). XRDI has only recently been applied to monolike silicon and solar cells. Rocking curve imaging is a further refinement,

leading to quantitative maps of crystal deformation, as described below.

### How X-rays are generated by a synchrotron and in a sealed tube source

Synchrotron facilities are large and are usually operated at a national or international level for the benefit of academic and industrial users in the communities which finance them. There are many such facilities around the world. Access is typically open via

competitive proposal processes or by purchasing beam time (with or without scientific support) or a measurement service.

The spectrum from a 'bending magnet' source, such as BM05 at the ESRF, is several orders of magnitude more intense than that from a sealed tube and is smooth and continuous – a skewed bell shape extending from a few eV up to hundreds of keV. BM05's spectrum peaks at 17keV. Synchrotrons also offer 'wiggler' and 'undulator' beamlines, which are yet

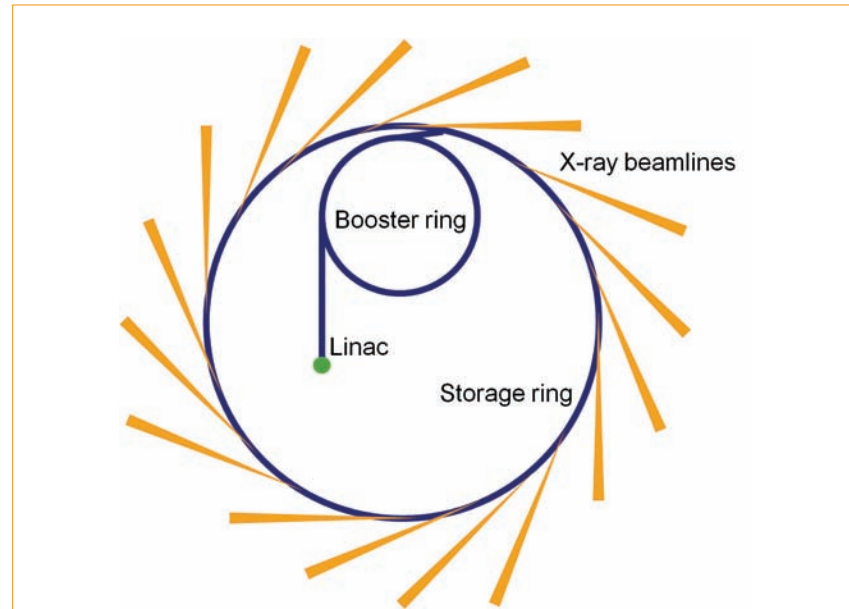


Figure 3. Schematic layout of a synchrotron. Electrons are generated at the start of the linear accelerator (Linac) and accelerated into the booster ring, where they are further accelerated before being injected into the storage ring at nearly the speed of light. When the electron trajectory is made to change direction (by magnetic fields), highly intense X-ray beams are generated in a forward direction. The ESRF has about 30 operational beamlines around a storage ring 844m in circumference.

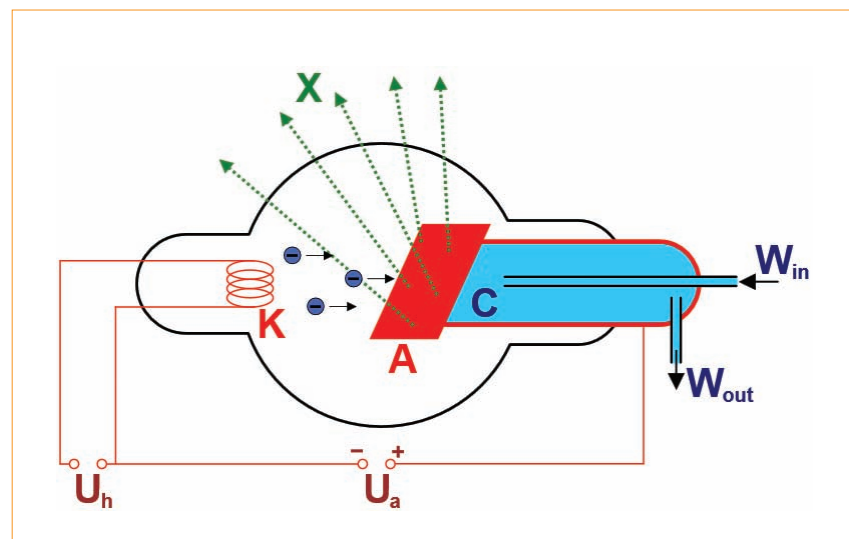


Figure 4. Diagram of a typical sealed tube X-ray source. Electrons are emitted by the heated cathode (K) and accelerated by a high voltage ( $U_a$ , typically  $\sim 40$ keV) to the anode (A), where they impinge, leading to the emission of X-rays (X). The anode is water cooled (W, C).

Credit: Image by Hmitch via Wikimedia Commons.

more intense, and give spectra with many peaks. Monochromation of a synchrotron beam thus offers a choice of beam energy over a wide range. The schematic layout of a synchrotron is shown in Fig. 3.

Compare this with a sealed tube X-ray source (Fig. 4). Electrons are generated in the same way, and accelerated to typically 30–50keV by an anode, which also serves as a target. The impinging electrons ionize atoms of the target material, leaving electrons at other energy levels to fall into the gaps, generating ‘characteristic X-rays’ at specific energies as they do so. Other impinging electrons are decelerated, giving rise to the broad continuum ‘Bremsstrahlung’ radiation at much lower intensity. The X-rays are emitted in all directions, and slits and windows are used to define the view of the source and its apparent divergence. The X-ray tube with its shielding assembly is less than 40cm in length and can be conveniently powered on or off as required by the user.

### How does XRDI work?

**XRDI at the synchrotron in white beam** BM05 allows a large, polychromatic (‘white’) beam to impinge on the sample. The different sets of atomic planes in the crystal select appropriate energies at appropriate diffraction angles (see Fig. 5) according to Bragg’s Law (Fig. 1). With the use of a 2D detector, information on the quality of the crystal can be obtained from the detail within each spot. A perfect, strain-free crystal yields a uniformly illuminated, undistorted diffraction spot. Defects in or on the crystal – such as dislocations, inclusions and precipitates, stacking faults and surface scratches – locally distort the crystal lattice and give rise to *contrast*

in the diffraction spot. The pattern of the contrast is a ‘signature’ of the type of defect. An overall stress causes the sample to curve and distorts the shape of the diffraction spot. In transmission geometry (the beam passing through the sample rather than diffracting from the incident surface), the image originates from the entire examined volume of the sample. In reflection geometry, the resulting images are dominated by diffraction from the material in a region of several microns (typically ~5–50 $\mu\text{m}$ ) near the surface.

#### XRDI with a sealed tube

When imaging is performed with a sealed tube X-ray source, the near-monochromatic characteristic emission line is used, requiring appropriate orientation of the sample in order to produce a single diffraction spot. Only a line region diffracts at a given angular

and spatial position, so the sample is moved through the beam and either the image is integrated on photographic film or a series of digital images is stitched together afterwards to produce the complete topograph.

A comparison of white beam synchrotron XRDI and lab XRDI is presented in Table 1.

### What do we see with X-ray vision?

XRDI shows the distortions in a crystal lattice, and these traces can be linked back to the defect which caused them. Fig. 6 shows close-ups of synchrotron topographs of a Czochralski silicon (Cz-Si) wafer and a mono-like wafer. The Cz-Si wafer is practically defect free; in contrast, the mono-like wafer exhibits images of tangles of randomly oriented

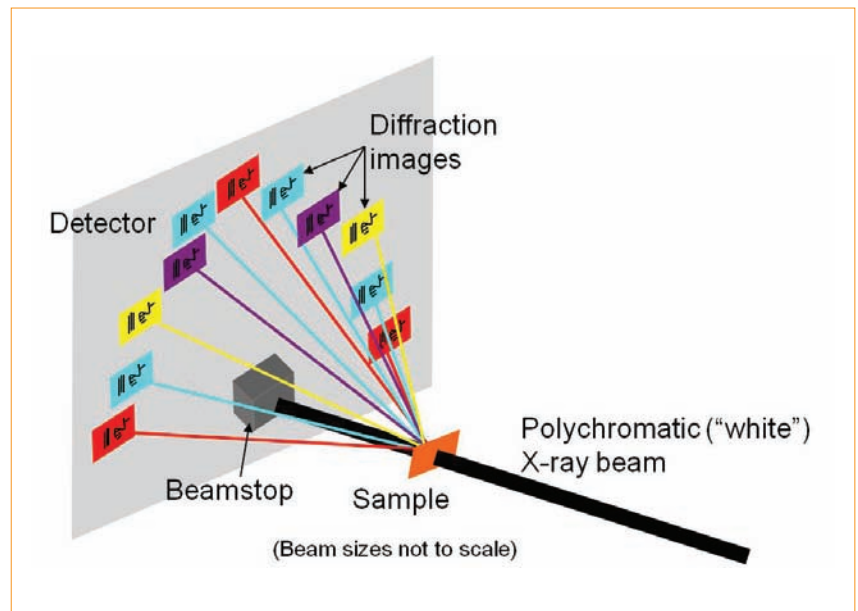


Figure 5. Illustration of white beam XRDI (topography) in transmission geometry.

	White beam synchrotron XRDI (BM05, ESRF)	Lab XRDI (Jordan Valley QC-TT)
Maximum topograph size	~100mm (H) $\times$ ~10mm (V) may be imaged in a single exposure; up to ~150mm (H) $\times$ ~100mm (V) by displacing the sample and stitching the images together	Samples up to 450mm diameter may be mounted and fully imaged with no edge loss
Incident beam	White beam (polychromatic): a few keV to more than 200keV; very low divergence (quasi-parallel)*	X-ray tube (predominantly monochromatic) – typically 8keV or 17keV, divergent
Sample planes imaged	Many, in different directions	One set of planes imaged per measurement
Image collection	Film for large area collection	Digital X-ray sensor with software image integration
Experimental geometric resolution	1 $\mu\text{m}$	6 $\mu\text{m}$
Image resolution	~5 $\mu\text{m}$ (film)	75 $\mu\text{m}$ in survey mode, 10 $\mu\text{m}$ in review mode
Typical measurement time	~0.1s exposure + a few minutes for film development	A few minutes for scanning + image stitching

\* The synchrotron beam may also be highly monochromated using appropriate beam optics. This is necessary for rocking curve imaging, discussed later, where high-resolution optics and camera systems are used for data collection, with sub-micron image pixel sizes attainable.

Table 1. Comparison of synchrotron and lab XRDI systems.

inter  
**solar**  
connecting solar business

DISCOVER THE  
WORLD OF INTERSOLAR



Intersolar Europe | Munich

Intersolar North America | San Francisco

Intersolar South America | São Paulo

Intersolar India | Mumbai

Intersolar China | Beijing

Intersolar Summits | Worldwide



Discover the  
world of Intersolar  
[www.intersolarglobal.com](http://www.intersolarglobal.com)

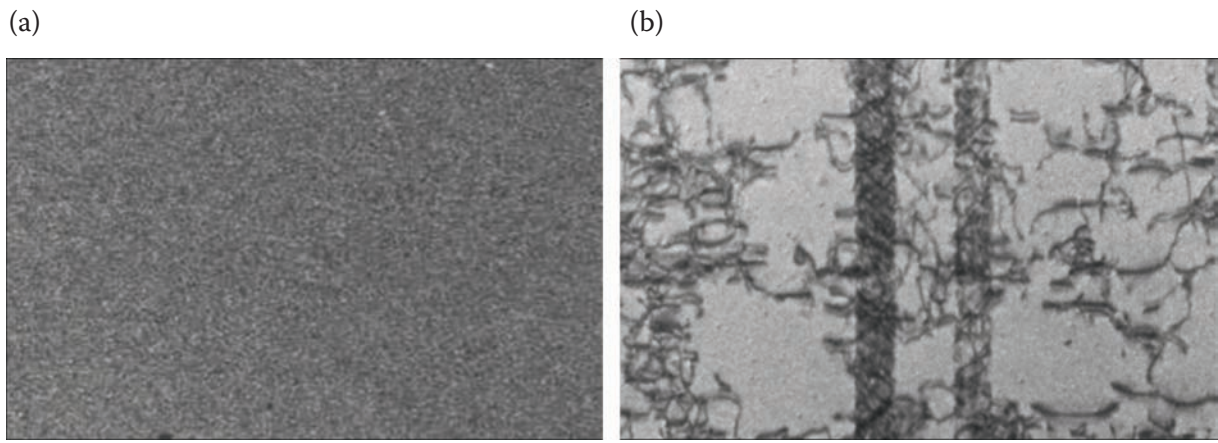


Figure 6. Topographs recorded by BM05: (a) close-up of XRDI of a Cz-Si sample, which is practically free of defects (graininess in the image is caused by the film emulsion); (b) the same type of image for a mono-like silicon sample. The observation of tangled dislocations is fairly typical, but it is unusual to see the bands of parallel dislocations. (Height of images ~1mm.)

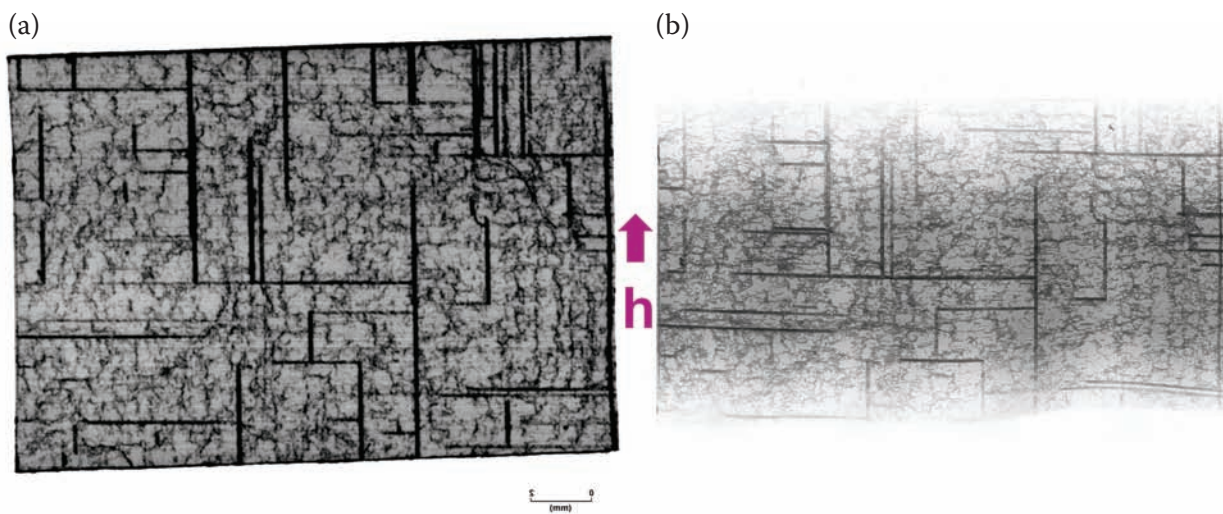


Figure 7. (a) Digital transmission topograph of the 220 planes of a mono-like silicon wafer sample, collected with the QC-TT; (b) the same measurement taken by BM05 using film, subsequently digitized using an optical microscope. (The scale bar is 2mm long, and  $h$  is the projection of the diffraction vector on the plane of the images.)

dislocations, as well as straight bands consisting of parallel dislocations running through the thickness of the sample, lying on particular crystallographic planes. These bands were observed to run through neighbouring wafers, and are unusual in mono-like samples – in the vast majority of cases, only tangles of dislocations are observed. There is no evidence of precipitates in this sample. Precipitates sometimes get caught at grain boundaries, and may be sources of dislocations. Control of growth conditions to minimize or control the generation and multiplication of dislocations, grain boundaries and precipitates is the subject of much study in the PV R&D community, as these can all reduce PV performance (e.g. [1–3]).

### “XRDI shows the distortions in a crystal lattice.”

Fig. 7 compares XRDI images of a mono-like Si sample 20mm × 15mm, taken by the QC-TT and at the synchrotron. The main features are evident in the images from both methods – straight lines of dislocations, as well as tangles. There are some differences to note, however:

- Slight misorientations notwithstanding, the two images are not the same shape. This is because:
  - In the QC-TT, diffraction is obtained from the whole width of the sample, then the sample is scanned and the image stitched together. This image therefore more faithfully represents the

physical dimensions of the sample.

- The synchrotron image is a single exposure. The beam covers the width of the sample but not the full height, so not all of the sample is imaged in a single shot. However, multiple exposures may be collected and stitched together after digital scanning, if required.
- Curvature of the sample effectively focuses or defocuses the diffracted synchrotron beam in the direction of the diffraction vector. The dimensions of the diffraction spot compared with the area of the sample illuminated can be used to calculate the sample curvature
- In addition, the equipment used at BM05 holds the sample in a clamp at the bottom. This

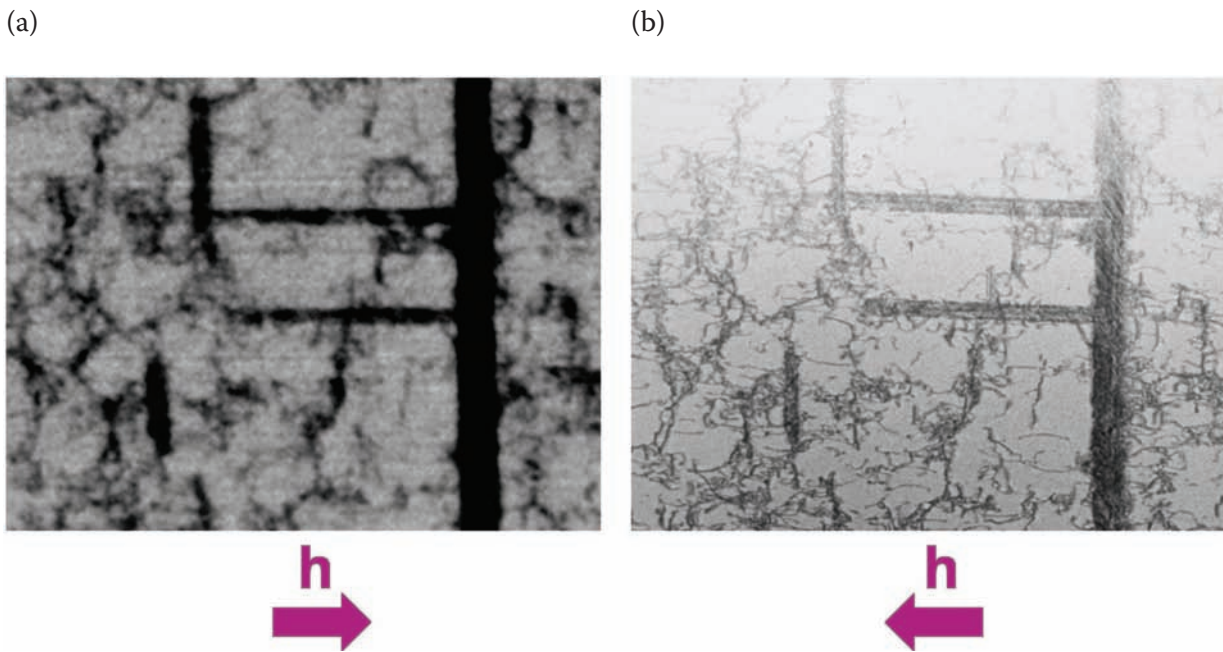


Figure 8. Zoom-in on other topographs of the mono-like Si sample shown in Fig. 7: (a) QC-TT image; (b) synchrotron image, showing sharper dislocation images and resolving the straight bands into groups of parallel dislocations running through the thickness of the sample. (Each image is approximately 4mm across, and  $h$  is the projection of the diffraction vector on the plane of the image.)

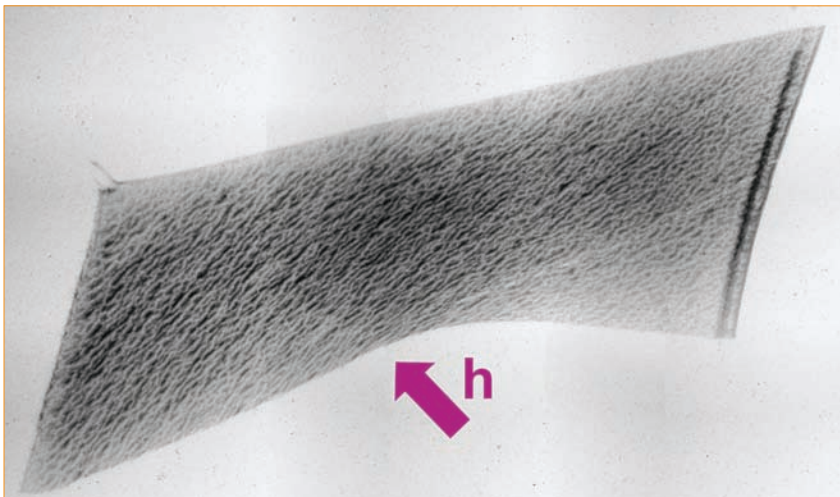


Figure 9. Synchrotron white beam topograph of a mono-like silicon sample with aluminium back-plane but no silver contact lines. The image is dominated by the 'orange-peel' effect of inhomogeneous distortions induced in the silicon by the back-plane.

shadows that part of the sample and, if the clamping is a little tight, also introduces strain, which locally distorts the image.

- The illumination is more uniform in the QC-TT image, owing to a more uniform diffraction line (which is then scanned) and to subsequent image processing. No image processing has been applied to the synchrotron data here, and the beam intensity profile in the vertical direction shows through.

The advantages of the synchrotron are evident in the finer details (Fig. 8). The lines of dislocations are revealed to consist of 'walls' of parallel dislocations passing from one surface of the sample to the other. The inherent geometric resolution of the BM05 experiment is around  $1\mu\text{m}$  in the white beam case, decreasing to  $0.1\mu\text{m}$  or lower when configured for a monochromatic beam. For the QC-TT, the resolution is  $6\mu\text{m}$ , coupled here with a  $10\mu\text{m}$  pixel camera. That said, the widths of features in the images are often tens or hundreds

of micrometres, which is determined by the width of the strained crystal regions around the defects and by the measurement configuration.

In addition to taking measurements on bare wafers, XRD can be applied at any stage of the processing, through to the final solar cell structure. In the case of conventional-architecture p-type silicon solar cells, the images are dominated by an 'orange-peel' effect arising from the inhomogeneous strain induced in the silicon by the screen-printed aluminium back-plane contact, which is co-fired along with the silver contact lines on the front face. Details of defects in the wafer itself are obscured. In addition, the Al back-plane induces bow in the silicon wafer, and the synchrotron white beam topographs are distorted in the direction of the diffraction vector – perpendicular to this, the images are not sensitive to distortion (Fig. 9). The distortion can be exploited to extract the sample curvature and stress.

### Quantitative detail via monochromatic beam XRD and rocking curve imaging

The extremely high intensity of the synchrotron beam, and the ability to monochromate it finely at the energy of choice using a crystal monochromator, gives access to a quantitative imaging technique called *rocking curve imaging* (RCI) [4,5]. With a single-energy X-ray beam incident on the sample, the

sample angle must be set precisely if the diffraction condition is to be met. The sample can then be scanned around this angle. The ‘rocking curve’ is the plot of diffracted intensity vs. angle.

Instead of measuring a single value of intensity and integrating while the sample angle is scanned, individual images are collected at different angular positions across the rocking curve using an optics and charge-coupled device (CCD) system. Considering all the images as if superposed in a stack, each pixel, looking through the stack, contains a local rocking curve. The

integrated intensity, the full width at half-maximum (FWHM) and the angular position of the diffraction peak can be extracted for each pixel, generating quantitative maps of the local sample crystalline quality (Fig. 10).

In addition, a comparison of images from diffraction from different planes of atoms can identify the type of dislocations (screw, edge or mixed) and the planes affected by them – useful information, since not all dislocations are necessarily electrically active. If the sample is not too distorted, individual pixels map directly to physical locations on the sample.

“To obtain depth resolution, section topography is employed.”

However, there is no information in such an image about where in the thickness of the examined sample lies the defect; to obtain depth resolution, section topography is employed (Fig. 11). With BM05, multiple beams – each 10 $\mu\text{m}$  wide – facilitate multiple sections in a single data collection. The QC-TT offers a single beam, typically

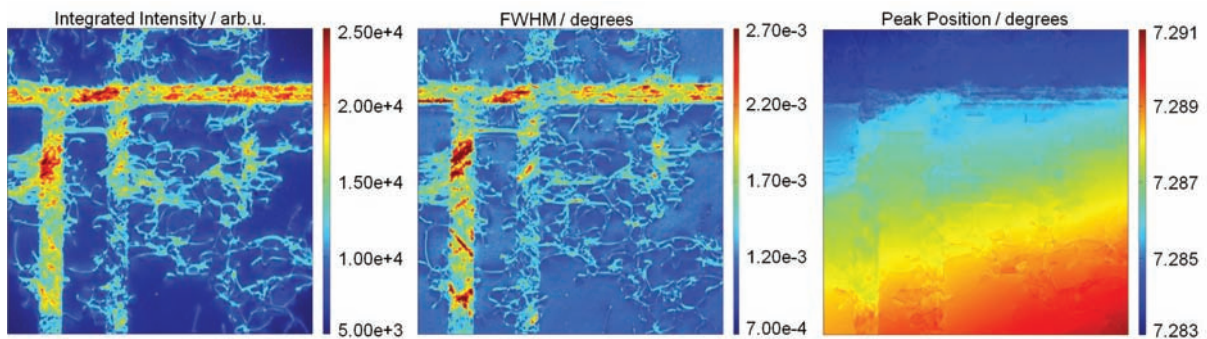


Figure 10. Maps of three rocking curve parameters, indicators of sample quality, showing defect behaviour and extracted from an RCI data set. (Images 1.5mm across; image pixel size 0.75 $\mu\text{m}$ ; mono-like silicon; diffraction vector vertical upwards.)

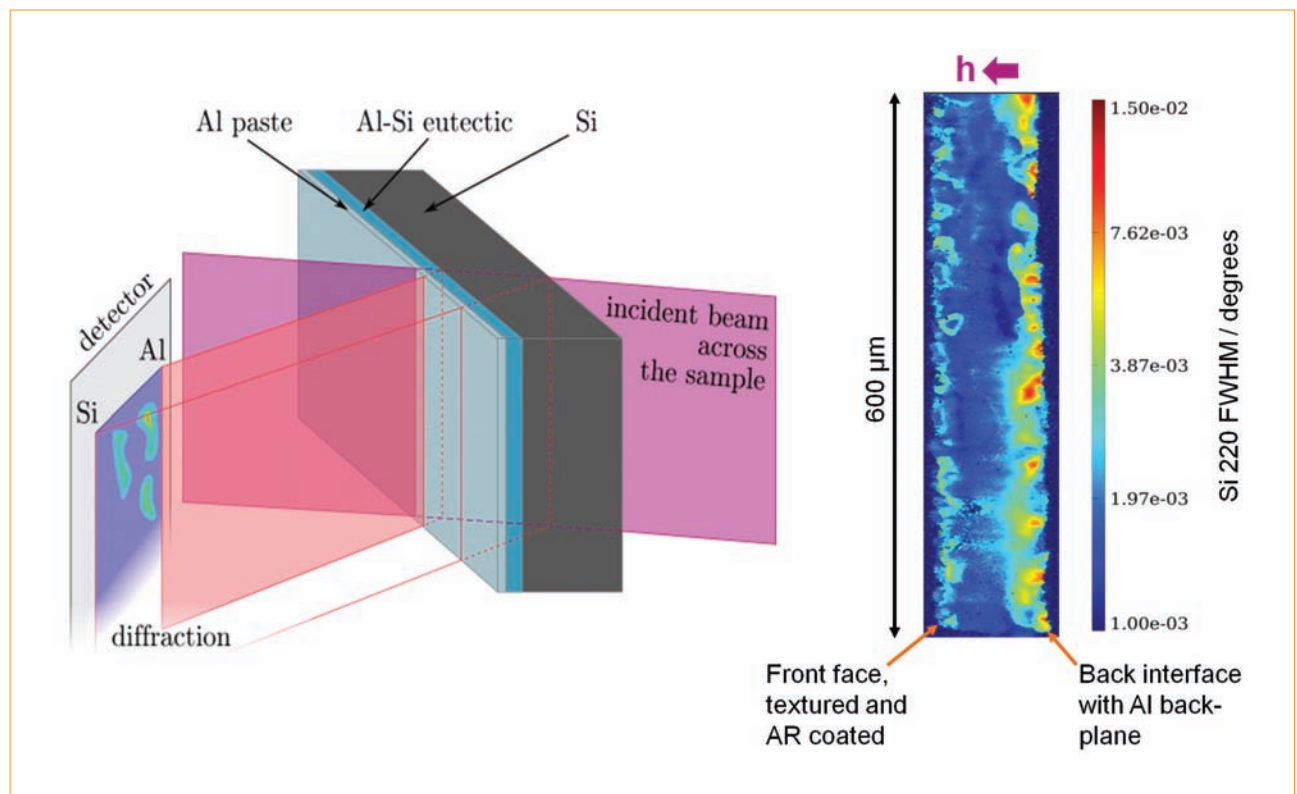


Figure 11. (a) Schematic of section topography; (b) close-up of a synchrotron section topograph of a mono-like Si sample with an Al back-plane. Only the silicon diffracts, so just the effects on the silicon of the back-plane and of the front-surface texturing, doping and anti-reflective coating are seen – not the effect on the actual back-plane or texturing. Greater distortion gradients show up in the larger diffraction peak FWHM values. (The image width corresponds to the silicon thickness of  $\sim 200\mu\text{m}$ .)



**Figure 12.** Depth-selective images from the QC-TT, generated from the same measurement data set: (a) back of a mono-like Si sample; (b) front of the sample. The red ellipses indicate some features which are not common to the two images and therefore arise from defects located at or near the respective surfaces.

50 $\mu$ m wide, via an adjustable slit system. The narrow region of the sample intersected by the X-ray beam diffracts, giving a virtual, non-destructive, slice view through the sample and thus of the distribution of defects through its thickness. This also enables meaningful measurements to be performed on full solar cell structures, getting around the ‘orange-peel’ effect induced by metallic back-planes, which dominates projection images [6,7].

In the example shown in Fig. 11, the combination of surface texturing, anti-reflective coating and local doping causes distortion gradients at the front side of the silicon. In the centre of the wafer, the silicon quality is near perfect in places (the FWHM approaches the instrumental limit for the configuration used), while much higher, further-reaching distortions are induced by the Al back-plane, which, on annealing, has generated a p<sup>+</sup> Al-doped layer and an Al-Si eutectic layer as well as the inhomogeneous Al back contact.

Alternatively, thanks to the digital imaging technique used in the QC-TT, some depth information can be accessed via the way the original images are processed. Scanning topography collects a series of adjacent cross sections across the area of the sample. Rather than stitch the entirety of every cross-section image together, a region of interest (RoI) can be selected corresponding to a particular

depth range through the sample. Stitching these RoIs together creates a top-down view of the sample area at a given depth, in contrast to the section topograph, which gives a virtual slice through the thickness at a given position.

Fig. 12(a) shows the back and Fig. 12(b) the front of a mono-like Si sample. Many features are common between the two images, which means that these features exist throughout the whole sample thickness; however, some are clearly stronger in one image or the other, indicating that they are at the front or back surface (examples marked with ellipses). On the image of the back of the sample (Fig. 12(a)), there are two dark spots (possibly arising from inclusions, precipitates or surface damage) that do not show up on the front image (Fig. 12(b)); moreover, on the front surface there is a scratch that is not on the back.

### That is not all that X-ray vision can reveal

Other X-ray techniques are also useful for examining material for solar cells, from bare wafers through to full cell structures. Nano-X-ray diffraction (n-XRD) enables additional quantitative detail of the crystal distortion to be probed [7]. Also, the fact that X-rays (like sunlight) are photons means that they too provoke

a PV response in a cell; this allows the simultaneous measurement of local defects and their effect on PV performance, as in the case of nano-X-ray fluorescence studies (e.g. [2,3,8]), which correlate local impurities with pre-breakdown sites and non-uniformity of the PV response.

**“XRDI gives unique insights into crystalline structure and its defects in a non-destructive way.”**

### Conclusions

XRDI gives unique insights into crystalline structure and its defects in a non-destructive way. It is applicable to samples ranging from bare material (and not restricted to silicon) to full cell structures, requiring only that the sample be predominantly monocrystalline in the area investigated. Information can be obtained by using either a lab system or a synchrotron, with each having benefits. The lab system can be applied in the production line, as clean-room compatible equipment is commercially available, and could be used to screen and select samples for measurement at a synchrotron facility, where higher spatial resolution XRDI or rocking curve analysis can be performed for more in-depth investigations.

### Acknowledgements

Thanks to S. Dubois of the CEA-INES for the samples (under a collaboration between the CEA-INES and the ESRF), and to T.N. Tran Thi for the images in Figs. 9 and 11.

### References

- [1] Tsoutsouva, M.G. et al. 2014, "Segregation, precipitation and dislocation generation between seeds in directionally solidified mono-like silicon for photovoltaic applications", *J. Cryst. Growth*, pp. 397–403 (doi:10.1016/j.jcrysgro.2013.12.022).
- [2] Kwapil, W. et al. 2009, "Observation of metal precipitates at prebreakdown sites in multicrystalline silicon solar cells", *Appl. Phys. Lett.*, Vol. 95, pp. 232113-1–232113-3.
- [3] Buonassi, T. et al. 2005, "Quantifying the effect of metal-rich precipitates on minority carrier diffusion length in multicrystalline silicon using synchrotron-based spectrally resolved x-ray beam-induced current", *Appl. Phys. Lett.*, Vol. 87, pp. 044101-1–044101-3
- [4] Lübbert, D. et al. 2000, "µm-resolved high resolution X-ray diffraction imaging for semiconductor quality control", *Nucl. Instr. Meth. Phys. Res. B*, Vol. 160, pp. 521–527.
- [5] Lübbert, D. et al. 2005, "Distribution and Burgers vectors of dislocations in semiconductor wafers investigated by rocking-curve imaging", *J. Appl. Cryst.*, Vol. 38, pp. 91–96.
- [6] Lafford, T.A. et al. 2013, "Synchrotron X-ray imaging applied to solar photovoltaic silicon", *J. Phys.: Conf. Series*, Vol. 425, pp. 192019-1–192019-4 (doi:10.1088/1742-6596/425/19/192019).
- [7] Tran Thi, T.N. et al. 2014, "Czochralski and mono-like p-type and n-type silicon solar cells: Relationship between strain and stress induced by the back contact, and photovoltaic performance", *Solar Energy Mater. & Solar Cells* [submitted for publication].
- [8] Villanova, J. et al. 2012, "Synchrotron microanalysis techniques applied to potential photovoltaic materials", *J. Synchrotron Rad.*, Vol. 19, pp. 521–524.

### About the Authors



**Tamzin Lafford** is a beamline scientist/ industrial liaison scientist for BM05 at the ESRF, having previously spent several years working in industry on X-ray characterization. Her research interests centre on XRDI applied to silicon for solar cells, from bare wafers to full structures. This has been carried out in collaboration with the CEA-INES (Institut National pour l'Énergie Solaire), where, together with industrial partners, cutting-edge and applied research is combined with innovation.



**Richard Bytheway** is a technologist at Jordan Valley Semiconductors UK Ltd., where he has spent 13 years developing X-ray metrology instruments. He previously worked in the fields of laser diffraction and geotechnical metrology, and is currently involved in applications development of the XRDI tools.



**Daniel Bright** is an applications engineer at Jordan Valley Semiconductors UK Ltd., specializing in X-ray topography. He has been developing XRDI methods and instruments for two years, as well as working on applications development of the XRDI tools.

### Enquiries

Tamzin Lafford  
ESRF  
71 Avenue des Martyrs  
CS 40220  
38043 Grenoble Cedex 9  
France  
Email: tamzin.lafford@esrf.fr  
Website: www.esrf.eu

Richard Bytheway  
Jordan Valley Semiconductors UK Ltd.  
Belmont Business Park  
Durham DH1 1TW, UK  
Email: richard.bytheway@jvsemi.co.uk  
Website: www.jvsemi.com